Focusing of high numerical aperture cylindrical-vector beams

K. S. Youngworth and T. G. Brown

The Institute of Optics, University of Rochester, Rochester, New York 14627

worth@optics.rochester.edu

Abstract: Cylindrical-vector beams are of increasing recent interest for their role in novel laser resonators and their applications to electron acceleration and scanning microscopy. In this paper, we calculate cylindrical-vector fields, near the focal region of an aplanatic lens, and briefly discuss some applications. We show that, in the particular case of a tightly focused, radially polarized beam, the polarization shows large inhomogeneities in the focal region, while the azimuthally polarized beam is purely transverse even at very high numerical apertures.

OCIS codes: (110.2990) Image formation theory; (140.3300) Laser beam shaping; (260.5430) Polarization

References and links

1. B. Richards and E. Wolf, "Electromagnetic diffraction in optical systems II. Structure of the image field in an aplanatic system," Proc. Roy. Soc. A **253**, 358-379 (1959).
2. A. Boivin and E. Wolf, "Electromagnetic field in the neighborhood of the focus of a coherent beam," Phys. Rev. B **138**, 1561-1565 (1965).
3. A. Yoshida and T. Asakura, "Electromagnetic field near the focus of Gaussian beams," Optik **41**, 281-292 (1974).
4. A. Yoshida and T. Asakura, "Electromagnetic field in the focal plane of a coherent beam from a wide-angular annular-aperture system," Optik **40**, 322-331 (1974).
5. T. Wilson, R. Juskaitis, and P. Higdon, "The imaging of dielectric point scatterers in conventional and confocal polarisation microscopes," Opt. Commun. **141,** 298-313 (1997).
6. P. Török, P.D. Higdon, and T. Wilson, "On the general properties of polarised light conventional and confocal microscopes," **148**, 300-315 (1998).
7. T. Erdogan, O. King, G. W. Wicks, D. G. Hall, E. H. Anderson, and M. J. Rooks, "Circularly symmetrical operation of a concentric-circle-grating, surface-emitting, AlGaAs/GaAs Quantum-well semiconductor-laser," Appl. Phys. Lett. **60**, 1921-1923 (1992).
8. R. H. Jordan and D. G. Hall, "Free-space azimuthal paraxial wave equation: the azimuthal Bessel-Gauss beam solution," Opt. Lett. **19**, 427-429 (1994).
9. D. G. Hall, "Vector-beam solutions of Maxwell's wave equation," Opt. Lett. **21**, 9-11 (1996).
10. P. L. Greene and D. G. Hall, "Diffraction characteristics of the azimuthal Bessel-Gauss beam," J. Opt. Soc. Am. A **13**, 962-966 (1996).
11. P. L. Greene and D. G. Hall, "Properties and diffraction of vector Bessel-Gauss beams," J. Opt. Soc. Am. A **15,** 3020-3027 (1998).
12. P. L. Greene and D. G. Hall, "Focal shift in vector beams," Opt. Express **4**, 411-419 (1999), http://www.opticsexpress.org/tocv4n10.htm.
13. C. J. R. Sheppard and S. Saghafi, "Transverse-electric and transverse-magnetic beam modes beyond the paraxial approximation," Opt. Lett. **24,**1543-1545 (1999).

#22809 - $15.00 US Received May 26, 2000; Revised June 21, 2000

14. M. Stalder and M. Schadt, "Linearly polarized light with axial symmetry generated by liquid-crystal polarization converters," Opt. Lett. **21**, 1948-1949 (1996).
15. R. Yamaguchi, T. Nose, and S. Sato, "Liquid-crystal polarizers with axially symmetrical properties", Jpn. J. Appl. Phys. **28**, 1730-1731 (1989).
16. D. Pohl, "Operation of a ruby laser in the purely transverse electric mode TE_{01}," *Appl. Phys. Lett.* **20**, 266-267, 1972.
17. J. J. Wynne, "Generation of the rotationally symmetric TE_{01} and TM_{01} modes from a wavelength-tunable laser," IEEE J. Quant. Elec. **QE-10**, 125-127 (1974).
18. M. E. Marhic and E. Garmire, "Low-order TE_{0q} operation of a CO_2 laser for transmission through circular metallic waveguides," Appl. Phys. Lett. **38**, 743-745 (1981).
19. S. C. Tidwell, G. H. Kim, and W. D. Kimura, "Efficient radially polarized laser-beam generation with a double interferometer," Appl. Opt. **32**, 5222-5229 (1993).
20. S. C. Tidwell, D. H. Ford, and W. D. Kimura, "Generating radially polarized beams interferometrically," Appl. Opt. **29**, 2234-2239 (1990).
21. E. G. Churin, J. Hossfeld, and T. Tschudi, "Polarization Configurations with singular point formed by computer-generated holograms," Opt. Commun. **99**, 13-17 (1993).
22. K. S. Youngworth and T. G. Brown, "Inhomogeneous polarization in scanning optical microscopy," Proc. SPIE **3919** (2000)
23. B. Hecht, B. Sick, U. P. Wild, and L. Novotny, "Orientational imaging of single molecules by annular illumination," submitted to Phys. Rev. Lett.
24. J. Enderlein, "Theoretical study of detection of a dipole emitter through an objective with high numerical aperture," Opt. Lett. **25**, 634-636 (2000).
25. T. Ha, T. A. Laurence, D. S. Chemla, and S. Weiss, "Polarization spectroscopy of single fluorescent molecules," J. Phys. Chem. B **103**, 6839-6850 (1999).

1. Introduction

The three-dimensional distribution of focused electromagnetic fields is an interesting and important topic in both applied optics and optical physics. High numerical aperture (NA) focusing is used both in fundamental probes of matter and in applications such as confocal microscopy and optical data storage. Because such techniques often rely on light of known polarization, the vector nature of the focused beam is of paramount importance.

The basic machinery by which focused polarized beams can be analyzed was described by Richards and Wolf [1]. That, and most subsequent work (e.g., references [2]-[6]), considered only those cases in which the illumination in the pupil is uniformly polarized. In this paper, we consider two cases of spatially nonuniform polarization which are of recent and continuing interest in optics.

Of particular interest is illumination which is polarized in such a way as to perfectly preserve the axial symmetry of an optical system. There are two types of beams which may satisfy this: 1) Beams whose *electric field* is aligned in an azimuthal orientation with respect to the optical axis, and; 2) Beams whose *magnetic field* is aligned in an azimuthal orientation, with the electric field polarized in a radial direction. The former have been the subject of a number of papers by Hall and coworkers [7-12]. They constitute the lowest-order out-coupled radiation modes from a circularly symmetric DFB laser and, in free space, represent a family of solutions to the vector wave equation. The latter have been discussed in the general context of vector beams [9], but have not been analyzed in detail.

The paraxial form of the wave equation admits single-mode azimuthally-polarized Bessel-Gauss solutions. The propagation and focusing properties of these paraxial beams has been studied in some detail in several recent papers by Greene and Hall [10-12]. Sheppard

#22809 - $15.00 US Received May 26, 2000; Revised June 21, 2000

recently presented a corresponding class of nonparaxial vector solutions by identifying appropriate source-sink combinations [13]. (Indeed, one of the significant properties of the radial solutions is their close correspondence to the radiating field of a dipole oriented along the optical axis.) The beams have been investigated experimentally (e.g., references [14]-[21]), both in the aforementioned DFB laser work, and in the context of electron accelerator physics [20]. In a recent paper, we have described a simple experimental method of generating these beams from a linearly polarized source [22].

In this paper, we consider the behavior of such beams when focusing from a finite aperture in the nonparaxial limit. We consider both the transverse and longitudinal field distributions near focus, and briefly discuss some interesting applications. As expected, the azimuthally polarized beam is always transverse even under very tight focusing conditions. Of particular significance is the fact that the radially polarized beam acquires an on-axis longitudinal component that can considerably exceed the strength of the transverse component.

In section 2, the theoretical electric fields for radially and azimuthally polarized beams are derived. In section 3, specific examples of these beams and linearly polarized beams are presented using the same set of parameters for each illumination. Section 4 contains a discussion of some possible applications for these beams.

2. Theory

2.1 Geometry of the problem

Figure 1 illustrates the geometry of the problem, where we have adopted a similar notation to that of Richards and Wolf [1]. The incident field, which may have any prescribed spatial distribution of the electric field amplitude and polarization, is assumed to have a planar phase front at plane 0 which is the entrance pupil to the optical system. An aplanatic lens produces a converging, spherical wave at focal sphere 1 (which may be taken to represent the exit pupil)

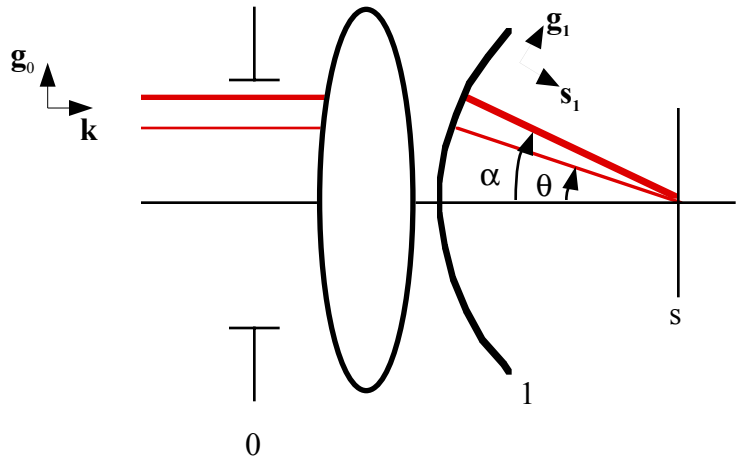

Fig. 1. Geometry of the problem. The input apodization is defined in plane 0, conjugate to focal sphere 1.

which propagates to a diffraction-limited axial point image (in the sample plane s) from a collimated source in region 0. The unit vector $\mathbf{g}_0$ is oriented perpendicular to the optical axis and has Cartesian components which may be expressed in cylindrical coordinates:

#22809 - $15.00 US
Received May 26, 2000; Revised June 21, 2000

$$\mathbf{g}_0 = \cos\phi\ \hat{\mathbf{i}} + \sin\phi\ \hat{\mathbf{j}}$$

where ϕ denotes the azimuthal angle with respect to the x-axis. Since $\mathbf{g}_0$ represents the radial component in object space, the azimuthal component may be denoted $\mathbf{g}_0 \times \hat{\mathbf{k}}$, where $\hat{\mathbf{k}}$ is a unit vector along z, the direction of propagation. The electric field in region 0 may then be resolved into its radial and azimuthal components:

$$\mathbf{e}_0 = l_0\left[e_r^{(0)}\mathbf{g}_0 + e_\phi^{(0)}\left(\mathbf{g}_0 \times \hat{\mathbf{k}}\right)\right], \tag{1}$$

in which l_0 denotes the relative amplitude of the field, which is assumed to vary radially but maintains cylindrical symmetry about the optical axis.

Following Richards and Wolf, we may express the electric field near focus as a diffraction integral over the vector field amplitude $\mathbf{a}_1$ on a spherical aperture of focal radius f_1.

$$\mathbf{e}^{(s)} = \frac{-ik}{2\pi}\iint_\Omega \mathbf{a}_1(\theta,\phi)\ e^{ik(\hat{\mathbf{s}}_1 \bullet \mathbf{r})}d\Omega \tag{2}$$

where the amplitude $\mathbf{a}_1$ may be related to the object space electric field as follows:

$$\mathbf{a}_1 = f_1 \cos^{1/2}(\theta)\ l_0(\theta)\left[e_r^{(0)}\mathbf{g}_1 + e_\phi^{(0)}\left(\mathbf{g}_1 \times \mathbf{s}_1\right)\right]. \tag{3}$$

The unit vector $\mathbf{g}_1$ lies in the plane containing both the ray and the optical axis and is perpendicular to $\hat{\mathbf{s}}_1$, the direction of propagation of the ray. If θ represents the polar angle, the radial unit vector may, after refraction, be expressed as

$$\mathbf{g}_1 = \cos\theta\left(\cos\phi\ \hat{\mathbf{i}} + \sin\phi\ \hat{\mathbf{j}}\right) + \sin\theta\ \hat{\mathbf{k}}. \tag{4}$$

We employ cylindrical coordinates $\mathbf{r} = (\rho_S, \phi_S, z_S)$ in image space, with origin $\rho_S = z_S = 0$ located at the paraxial focus. Then, for points near the paraxial focus,

$$\hat{\mathbf{s}}_1 \bullet \mathbf{r} = z_S\cos\theta + \rho_S\sin\theta\cos(\phi - \phi_S),$$

and suitable choice of the field amplitude $\mathbf{a}$ yields the electric field vector in the focal region.

2.2 Radially Polarized Illumination

For radially polarized illumination, we take $e_\phi^{(0)} = 0$ in equation (1). The Cartesian components of the electric field vector near focus may then be expressed as follows:

$$\mathbf{e}^{(s)} = \begin{bmatrix} e_x^{(s)} \\ e_y^{(s)} \\ e_z^{(s)} \end{bmatrix} = \frac{-iA}{\pi}\int_0^\alpha\int_0^{2\pi} \sin\theta\ \cos^{1/2}\theta\ l_0(\theta)\ e^{ik(z_S\cos\theta + \rho_S\sin\theta\cos(\phi-\phi_S))} \begin{bmatrix} \cos\theta\cos\phi \\ \cos\theta\sin\phi \\ \sin\theta \end{bmatrix} d\phi d\theta \tag{5}$$

Finally, we construct the local azimuthal and radial components of $\mathbf{e}^{(s)}$ through the following transformations:

$$\begin{aligned} e_\phi^{(s)} &= e_y^{(s)}\cos\phi_S - e_x^{(s)}\sin\phi_S \\ e_\rho^{(s)} &= e_x^{(s)}\cos\phi_S + e_y^{(s)}\sin\phi_S \end{aligned} \tag{6}$$

For this case, it is trivial to show that the azimuthal component is zero everywhere in image space. We therefore turn our attention to the radial and longitudinal components:

$$\begin{aligned} e_\rho^{(s)} &= \frac{-iA}{\pi}\int_0^\alpha\int_0^{2\pi} \cos^{1/2}\theta\ \sin\theta\ \cos\theta\ \cos(\phi-\phi_S)\ l_0(\theta)\ e^{ik(z_S\cos\theta + \rho_S\sin\theta\cos(\phi-\phi_S))}d\phi d\theta \\ e_z^{(s)} &= \frac{-iA}{\pi}\int_0^\alpha\int_0^{2\pi} \cos^{1/2}\theta\ \sin^2\theta\ l_0(\theta)\ e^{ik(z_S\cos\theta + \rho_S\sin\theta\cos(\phi-\phi_S))}d\phi d\theta \end{aligned} \tag{7}$$

The integrations over ϕ can be accomplished using the identity:

$$\int_0^{2\pi}\cos(n\phi)e^{ik\rho_P\sin\theta\cos\phi}d\phi = 2\pi i^n J_n(k\rho_P\sin\theta),$$

Where $J_n(k\rho_S\sin\theta)$ denotes a Bessel function of the first kind, of order n. For a pupil illuminated by radial polarization, the electric fields near focus then have the following form:

#22809 - $15.00 US
Received May 26, 2000; Revised June 21, 2000

$$e_{\rho}^{(s)}(\rho_S, z_S) = A\int_0^{\alpha} \cos^{1/2}\theta \sin(2\theta) l_0(\theta) J_1(k\rho_S \sin\theta) e^{ikz_S\cos\theta} d\theta$$
$$e_{z}^{(s)}(\rho_S, z_S) = 2iA\int_0^{\alpha} \cos^{1/2}\theta \sin^2\theta l_0(\theta) J_0(k\rho_S \sin\theta) e^{ikz_S\cos\theta} d\theta \quad (8)$$

It may readily be verified that, just as with the paraxial solutions, the radially illuminated objective produces a focal region with an on-axis null at all distances z_s from the paraxial focus.

2.3 Azimuthally polarized illumination

For azimuthally polarized illumination, we take $e_{\rho}^{(0)} = 0$ in equation (1). The Cartesian components of the electric field vector near focus may, in this case, be expressed as follows:

$$\mathbf{e}^{(s)} = \begin{bmatrix} e_x^{(s)} \\ e_y^{(s)} \\ e_z^{(s)} \end{bmatrix} = \frac{-iA}{\pi}\int_0^{\alpha}\int_0^{2\pi} \sin\theta \cos^{1/2}\theta\, l_0(\theta)\, e^{ik(z_S\cos\theta+\rho_S\sin\theta\cos(\phi-\phi_S))} \begin{bmatrix} -\sin\phi \\ \cos\phi \\ 0 \end{bmatrix} d\phi d\theta \quad (9)$$

Using the transformation of equation (6), the local radial and longitudinal components integrate to zero. The azimuthal component can be expressed:

$$e_{\phi}^{(s)} = \frac{-iA}{\pi}\int_0^{\alpha}\int_0^{2\pi} \cos^{1/2}\theta \sin\theta \cos(\phi-\phi_S) l_0(\theta)\, e^{ik(z_S\cos\theta+\rho_S\sin\theta\cos(\phi-\phi_S))} d\phi d\theta$$

The integrations over ϕ can be accomplished as before, yielding:

$$e_{\phi}^{(s)}(\rho_S, z_S) = 2A\int_0^{\alpha} \cos^{1/2}\theta \sin\theta\, l_0(\theta)\, J_1(k\rho_S \sin\theta) e^{ikz_S\cos\theta} d\theta \quad (10)$$

Just as with radial polarization, the azimuthally illuminated objective produces a focal region with an on-axis null at all distances z_s from the paraxial focus. As expected, and in a manner consistent with Maxwell's equations, the azimuthal field propagates as a purely transverse polarization through the entire focal region.

3. Example

One can, in principle, choose any prescribed apodization function $l_0(\theta)$ by using an appropriate pupil filter. A full discussion of the optimum apodization function is beyond the scope of this paper; for this example, we use the Bessel-Gauss solution of Jordan and Hall [8], and the procedure described in Youngworth and Brown [22] to obtain the electric field for radial and azimuthal polarization in the paraxial region. We assume a Bessel-Gauss beam waist at plane 0 to obtain:

$$l_0(\theta) = \exp\left[-\beta_0^2\left(\frac{\sin\theta}{\sin\alpha}\right)^2\right] J_1\left(2\beta_0\frac{\sin\theta}{\sin\alpha}\right) \quad (11)$$

where β_0 is the ratio of the pupil radius and the beam waist. We can then solve the resulting integrals (8) and (10) numerically and plot the intensities near focus for any numerical aperture. For this example we used an NA of 1.32 and an index of refraction (n) of 1.518 between the lens and the sample. These numbers are typical of a high-NA oil immersion microscope objective. All length measurements are in units of wavelengths, therefore, $\lambda = 1$; $\beta_0 = 3/2$, $A = 1$, $k = 2\pi/\lambda$, and $\alpha = \sin^{-1}(\mathrm{NA/n})$.

3.1 Radially Polarized Illumination

Figure 2 shows the intensity ($\mathbf{I} = |\mathbf{e}|^2$) of the transverse electric field at focus (X-Y plane) and through focus (ρ-Z plane). The on-axis energy null and annular intensity distribution, characteristics of axially symmetric beams, are apparent. Opposite sides of the beam are out of phase which causes the null to remain as the beam propagates. This phase relationship is

#22809 - $15.00 US
Received May 26, 2000; Revised June 21, 2000

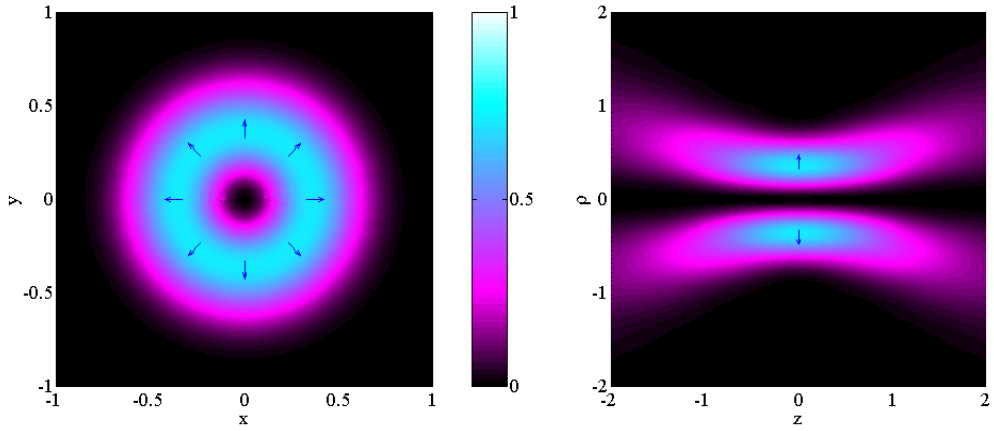

Fig. 2. Normalized intensity of the transverse (radial) component of a high-NA (1.32) radially polarized beam at focus and through focus. Intensities of 0 and 1 correspond to black and white, respectively. The units of x, y, ρ, and z are in wavelengths.

shown by the arrows. The *total* electric field is, of course, the vector sum of the transverse and longitudinal components. Figure 3 shows the intensity of the longitudinal electric field at focus (X-Y plane) and through focus (ρ-Z plane). The electric field points along the axis of propagation (shown with an arrow) and is strongest on axis. The intensity of the ring around the center lobe is very small compared to the maximum intensity, and it has a phase opposite the phase of the central lobe. As is the case with uniformly polarized beams, the point spread function (PSF) is wider in the longitudinal direction than in the transverse direction.

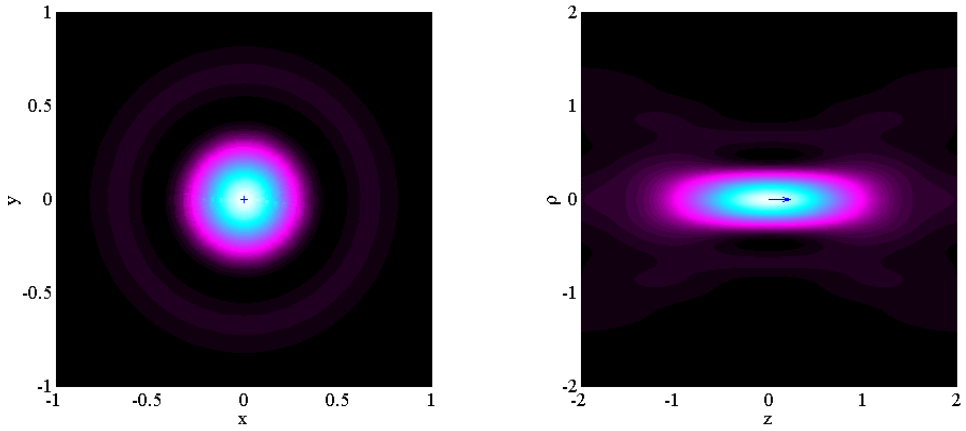

Fig. 3. Normalized intensity of the longitudinal (z-) component of a high-NA (1.32) radially polarized beam at focus and through focus. Intensities of 0 and 1 correspond to black and white, respectively. The units of x, y, ρ, and z are in wavelengths.

As the NA increases, the longitudinal field becomes stronger than the transverse field. This trend is shown in Figure 4 which displays the plot for the ratio of the maximum intensities of the longitudinal and transverse fields versus the focusing angle. We chose values for the NA ranging from 0.1 to 1.5 (for oil-immersion), and from 0.1 to 1 (for air), so α ranges from 0.0659 radians to $\pi/2$ radians. The results for air and oil are indistinguishable; the ratio of intensities therefore depends entirely on the focusing angle and not significantly on the index of refraction between the lens and the sample. At focusing

#22809 - $15.00 US
Received May 26, 2000; Revised June 21, 2000

angles greater than about 0.9 (NA values of about 0.8 in air and 1.2 in oil), the maximum longitudinal intensity becomes larger than the maximum transverse intensity. For the examples of Figures 2 and 3 the ratio is 1.4.

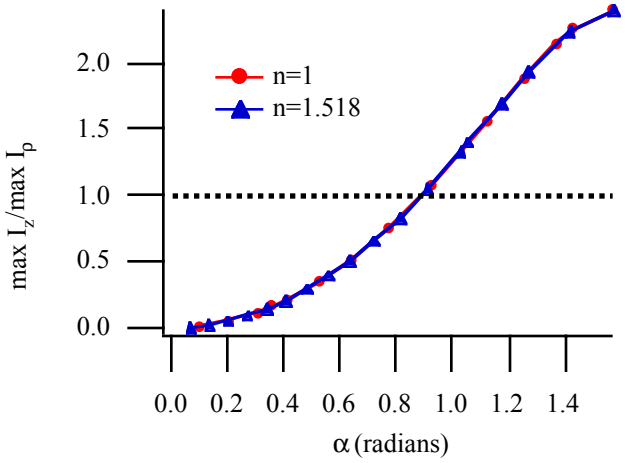

Fig. 4. The ratio of the maximum intensities of the longitudinal (max I_Z) and radial transverse (max I_ρ) fields versus the focusing angle (α). The dotted line shows where max I_Z becomes larger than max I_ρ. For the example, we used an objective with NA=1.32 in oil, or $\alpha \approx 1.05$ radians; max I_Z is 1.4 times larger than max I_ρ.

3.2 Azimuthally-polarized illumination

Figure 5 shows the intensity of the transverse electric field at focus (XY plane) and through focus (ρ-Z plane). The field of the azimuthally polarized beam is similar to the transverse component of the radially polarized beam, except that the phase of the electric field is rotated by 90°. A notable difference between azimuthally and radially polarized beams is that the azimuthally polarized beam does not create a longitudinal component, and the total field is transverse.

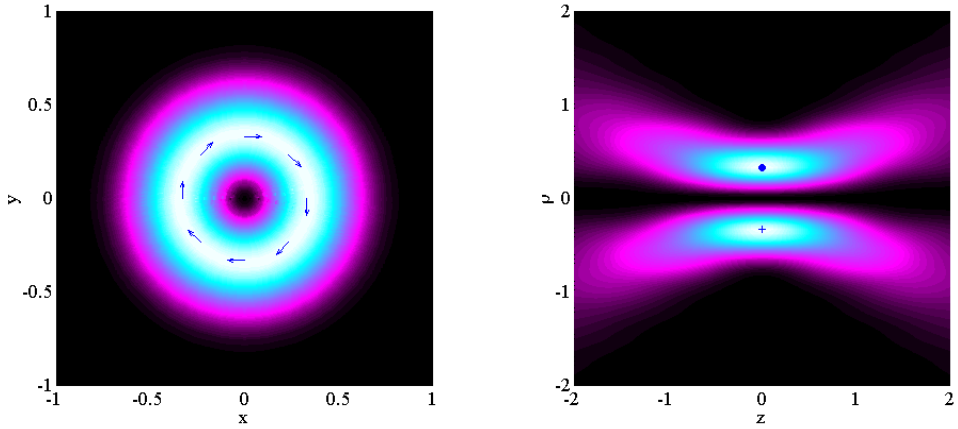

Fig. 5. Normalized intensity of the transverse (azimuthal) component of a high-NA (1.32) azimuthally polarized beam at focus and through focus. Intensities of 0 and 1 correspond to black and white, respectively. The units of x, y, ρ, and z are in wavelengths.

#22809 - $15.00 US
Received May 26, 2000; Revised June 21, 2000

3.3 Experimental Implementation

In our current experimental work we use an azimuthally polarized beam for the illumination in a scanning microscope. The method that we used to produce both this beam and its radially polarized counterpart employs a Mach-Zehnder interferometer equipped with polarization beamsplitters and a pair of π phase shifters, and is described in reference [22]. The entering beam undergoes a two-dimensional raster scan (controlled by a computer), followed by a beam expanding telescope which is designed to provide stationary pupil illumination. The microscope is a modified Leitz-Wetzlar design equipped with 5x, 10x, 25x, 40x, 60x, and 100x objectives and is used in reflection mode. The reflected beam is sent into the detection arm by a beam splitter. In the dark-field confocal (IPC) mode, a pinhole (smaller than the axial null) blocks all but the axial (scattered) light. The light is detected by a photomultiplier tube which sends signals to a computer to create an image. Figure 6 shows a movie of the beam as it appears before entering the microscope. The first part of the movie shows the beam with a linear polarizer (oriented from the upper left corner to the lower right corner) placed before the camera. In the second part, the polarizer is rotated clockwise, counterclockwise, and clockwise again; the rotating lobes on each side of the polarizer indicate that the beam is azimuthally polarized. In the third part, the polarizer is removed so that the annular shape of the beam can be seen. The movie of the radially polarized beam looks exactly the same, except for the orientation of the lobes with respect to the polarizer.

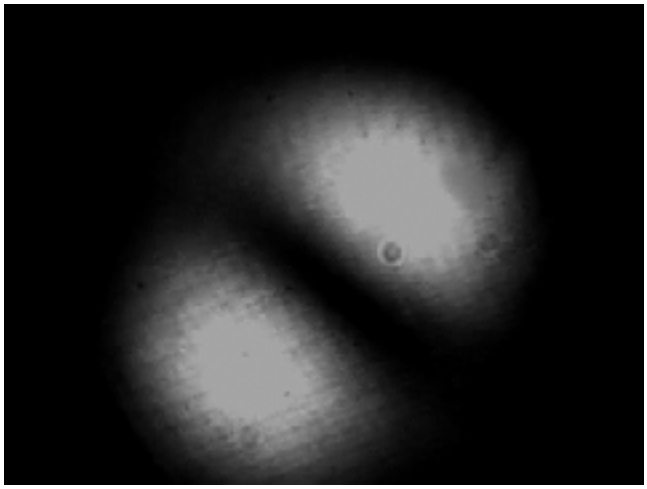

Fig. 6. Movie (2.1 MB) of an azimuthally polarized beam that was created by using a modified Mach-Zehnder interferometer to convert linear polarization to azimuthal polarization.

Inhomogeneously polarized illumination in confocal microscopy can be applied to semiconductor inspection by conventional methods [22]. Figure 7 shows a dark-field confocal image of a small scatterer on a metalized region of a silicon integrated circuit, taken with azimuthally polarized illumination. Since small scatterers can be used as measures of the point spread function (PSF) of the system, we see that the lateral PSF shows the expected annular shape of Figure 5. We see many fruitful experiments ahead with both polarizations.

#22809 - $15.00 US Received May 26, 2000; Revised June 21, 2000

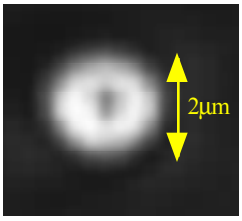

Fig. 7. A small scatterer on a metalized region of a silicon integrated circuit taken in dark-field confocal (IPC) mode with azimuthal polarization with a 40x (NA=0.65) objective.

3.4 Uniformly polarized illumination

It is helpful to compare images of the polarization distribution near focus to that of the well known case of a linearly polarized beam under similar conditions. This case was studied by Richards and Wolf (x-polarized) [1] and in the context of small particle microscopy, by Wilson, *et. al.* [5] and Török, *et. al.* [6]. Figures 8, 9, and 10 show the intensity of the transverse and longitudinal electric fields at focus (X-Y plane) of a linearly (y-) polarized beam. The beam is still largely polarized in the y-direction at focus (Figure 8), although this component is now slightly narrower in the x-direction at high numerical apertures [1]. Besides the original transverse component in the y-direction, a longitudinal component [2] is now present (Figure 9) which is about 7% of the peak intensity of the primary polarization, and is strongest near the y-axis on both side of the x-axis. There is also a transverse component in the x-direction (Figure 10) which is about 0.1% of the peak intensity of the primary polarization. It consists of four lobes, one in each quadrant of the XY plane. Quadrants I and III are in phase, and quadrants II and IV are of opposite phase. Experimental examples of these components are presented for isotropic scatterers by Wilson, *et. al.* [5] and Török, *et. al.* [6], and for single molecules by Hecht, *et. al.* [23].

Circularly polarized illumination is a linear combination of orthogonal, linearly polarized solutions. The longitudinal component in this case is of similar strength, but exhibits the annular distribution shown by Wilson, *et. al.* [5].

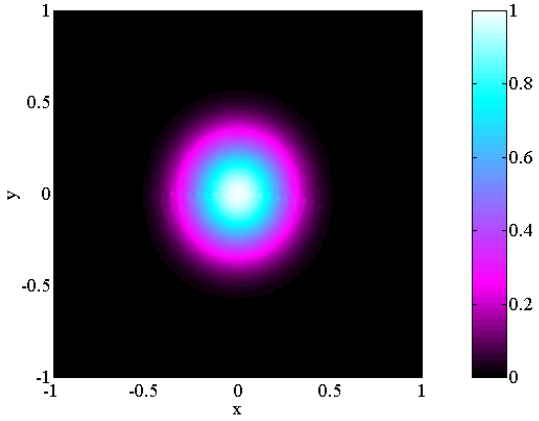

Fig. 8. Normalized intensity of the transverse (y-) component of a high-NA (1.32) linearly polarized beam. Intensities of 0 and 1 correspond to black and white, respectively. The units of x and y are in wavelengths.

#22809 - $15.00 US Received May 26, 2000; Revised June 21, 2000

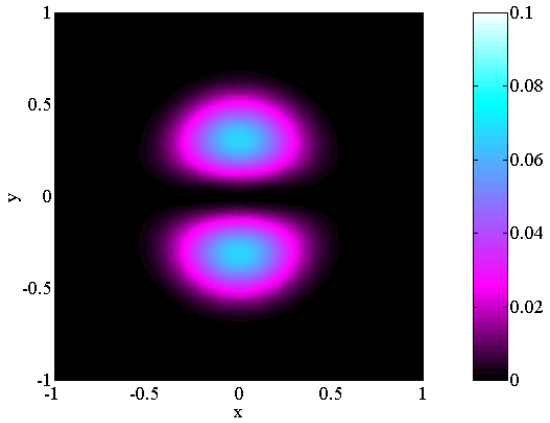

Fig. 9. Normalized intensity of the longitudinal (z-) component of a high-NA (1.32) linearly polarized beam. Note that the intensity is normalized from 0 to 0.1 instead of 0 to 1 as in previous figures. The units of x and y are in wavelengths.

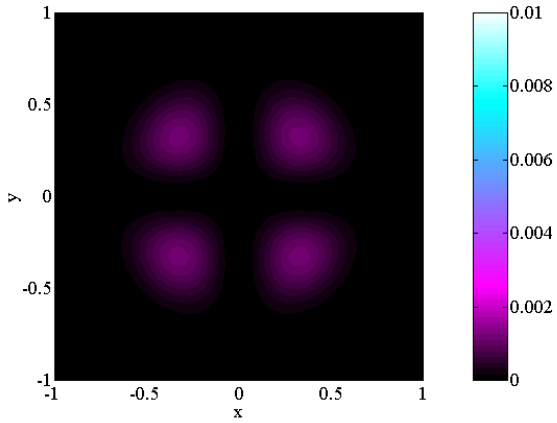

Fig. 10. Normalized intensity of the transverse (x-) component of a high-NA (1.32) linearly polarized beam. Note that the intensity is normalized from 0 to 0.01. The units of x and y are in wavelengths.

4. Discussion

Cylindrical-vector beams are distinguished by their spatially nonuniform polarization, the vector symmetry about the optical axis, and the ever-present on-axis null. Radially polarized beams also have a significantly stronger longitudinal field near focus than do uniformly polarized beams, whereas azimuthally polarized beams have no longitudinal field component. Yoshida [4], showed that by using annular illumination with linearly polarized light, the longitudinal component can be made stronger with respect to the transverse part; however, its maximum intensity is never larger than the transverse part's maximum intensity. These particular characteristics may be useful in applications (e.g., microscopy) where the field boundary conditions have a profound influence on particle or particle/surface interactions.

There is also interest in using longitudinal fields for purposes such as electron acceleration (e.g., references [2] and [20]) and near-field microscopy (e.g., references [23], [24], and [25]). For these applications, it is desirable to obtain the strongest longitudinal field possible. Since the radially polarized beam creates a significantly stronger longitudinal field

#22809 - $15.00 US
Received May 26, 2000; Revised June 21, 2000

than the uniformly polarized beam near focus, a radially polarized beam may be a better choice for the illumination.

Radially polarized illumination shows the unique property that, for each Cartesian coordinate, a strong field exists somewhere in the focused beam. At high NA, the z-field dominates in the center of the beam, whereas the x- and y-fields dominate away from the center on their respective axes. *Adjusting the numerical aperture allows one to define a focal region in which the electric field amplitude is nearly uniform throughout a focal volume, but whose orientation may vary over a full 2π steradians depending on location.*

5. Conclusion

In this paper we have calculated the electric fields of azimuthally and radially polarized beams near the focus of an aplanatic system. These equations will be the basis for future calculations that will model our experimental results (such as the image in Figure 7). By using an example that approximates a high numerical aperture microscope objective, we were able to show some of the significant differences between these beams and uniformly polarized beams. The radially polarized beam is distinguished by its strong longitudinal field at high numerical apertures. The azimuthally polarized beam is distinguished by a purely transverse annular focal region. Both have possible applications in scanning laser microscopy.

Acknowledgments

We are indebted to Professors Lukas Novotny, Dennis Hall, and Emil Wolf for helpful advice. This work was supported in part by the Semiconductor Research Corporation under contract 776.001.